Journal of Materials Chemistry C

Accepted Manuscript

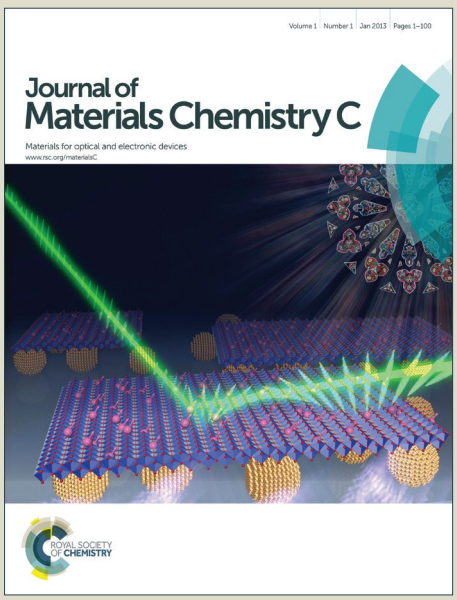

ROYAL SOCIETY OF CHEMISTRY

www.rsc.org/materialsC

Single p-n Homojunction White Light Emitting Diodes Based on High-performance Yellow Luminescence of Large-Scale GaN Microcubes

Bingbing Lv[1], Yingwen Tang[2], Shiyun Lou[*1], Yanling Xu[*3], Shaomin Zhou[*1]

[1]Key laboratory for Special Functional Materials of Ministry of Education, Henan University, Kaifeng 475004, China

[2]College of Physics and Information Engineering, Minnan Normal University, Zhangzhou 363000, China

[3]The Audit Department of Henan University, Kaifeng 475004, China

∗Corresponding authors: Tel: +86-371-22868833-3712; Fax: +86-371-23881358.

Cubic phase (zinc-blende) GaN (referred as c-GaN)-based phosphor-free white light emitting diodes (LEDs) can exhibit superior characteristics and ultrahigh efficiency compared with conditional hexagonal phase (wurtzite) GaN (referred as h-GaN)-based. However, one notorious issue is low quality of c-GaN due to thermodynamical instability of cubic phase, epilayer-substrate chemical incompatibility, and large lattice-mismatch during epitaxial deposition, giving rise to insufficient light emission efficiency. Therefore, improving quality of c-GaN is a key step towards high performance white LEDs. Here, we report the growth of high quality single crystalline GaN microcubes (MCs) with pure zinc-blende phase for large scale production by chemical vapor deposition method. From the GaN MCs, high-performance yellow luminescence (YL) is observed by different temperature photoluminescence spectra and the possible origin of the YL band is investigated. Furthermore, the fabricated phosphor-free single homojunction based on individual GaN MCs showed a diode nonlinear rectification behavior and the electroluminescence exhibited white emission when the operating voltage is 12 V. At room temperature, due to the reduction of threading dislocation density and the absence of piezoelectric polarization of the zinc-blend phase GaN, the device can exhibits an internal quantum efficiency of ~99.2% and virtually no efficiency droop as the injection current increases as well as an output power of ~4.4 mW for a typical operating current of 20 mA, which is approximately 50% stronger than that of conventional h-GaN homojunction LED.

* Corresponding author. e-mail: smzhou@henu.edu.cn

Introduction

As one of the most rapidly evolving branches of solid-state lighting technologies, LEDs are gradually replacing conventional lighting sources due to their advantages in energy saving and environmental protection[1-4]. At the present time, commercially available white LEDs are predominantly either rare-earth or inorganic-organic hybrid phosphor based[4]. However, the efficiency of this kind of white LED decreases rapidly as the phosphor used to convert blue to orange wavelength usually has a short lifetime and further the long-term reliability of the phosphors are additional detrimental factors[5, 6]. So, the top priority is development of all semiconductor-based large scale phosphor-free white LEDs that can exhibit ultrahigh efficiency, long-term reliability and tunable color emission[7-12]. In particular, most of phosphor-free white LEDs are based on nitride binaries and nitrogenous ternary alloys semiconductors[7, 13-15]. Among those nitride semiconductor materials such as GaN, AlN, BN, InGaN and AlGaN, GaN is the most promising candidate for use as functional building blocks in the efficient phosphor-free white LEDs due to its large band-gap, high optical absorption coefficient, high electron mobility, and low dielectric constant[16-18].

As we know, conventional GaN materials are hexagonal phase and possess very high polarization fields (~MV/cm) along the common growth direction of <001>. Such large polarization fields lead to undesired shifts such as wavelength and current in the performance of photonic and vertical transport electronic devices[10, 19-21]. The polarization effects can be eliminated by growing wurtzite nitride layers that their orientations include a-plane or m-plane of h-GaN. However, this is not very easy and their quality is still not excellent[22-25]. As a result, reduction of this built-in polar field is the main motivation for growing and studying c-GaN which is polarization-free along the common growth direction of c-axis[23, 26-28]. In recent years, cubic phase of GaN has been observed to form when grown on cubic substrates like GaAs or Al_2O_3[29-32]. However, due to the metastable nature of the cubic phase, epilayer-substrate chemical incompatibility and large lattice-mismatch make it difficult to grow pure c-GaN, the h-GaN composition frequently appeared in the growing c-GaN micro/nanostructure[23, 33-35]. Meanwhile, the low throughput or high cost associated with the techniques such as the molecular beam epitaxy[31], the hydride vapor phase epitaxy[32], and metalorganic chemical vapor deposition[30], limits the large-scale industrial production with inexpensive.

In this letter, in view of potential applications in optoelectronic devices, availability of cleavage and the

relatively low-cost of large diameter Si wafers, Si [(111) and (101)] is an interesting substrate to consider for GaN growth. Here, we report the growth of stress-free c-GaN MCs with 100% yield on Si (111) substrate by chemical vapor deposition (CVD), and the possible growth mechanism of the GaN MCs is discussed. Additional the optical investigations reveal high yellow-band emission performance from MCs, suggesting the potential application in luminescent devices. Based on as-obtained individual GaN MCs, we have further developed phosphor-free p-n homojunction white LED on Si (111) substrate. The strongest electroluminescence (EL) white emission from single p-n homojunction MC-based-LED (MC-LED) is observed at 12 V, which establishes the state-of-the-art c-GaN MCs optoelectronic devices. Compared with conventional h-GaN, the advantages including proper geometry for white-light emission as well as high luminous and power efficiency can be used for next-generation LEDs.

Experimental

Material Preparation and Characterization. GaN samples were directly synthesized using Ni as catalyst in a feasible CVD method, which is similar to our earlier work[1, 3, 36]. A polished Si wafer of 10×20 mm^2 was cleaned in 10% HCl solution for 30 min and rinsed with distilled water. We put the Si substrate coated with Ni as a catalyst by electron beam evaporation. The substrates were then patterned with Ni layer around 2 nm in thickness. Ga (99.999%) powders (1.5 g) were added in mortar and milled 30 min by manual operation at 25 °C. Then, the pure Ga powders were melted in a quartz crucible and the Si [(111) for MCs and (101) for GaN microhexahedrons (MHs)] substrate which deposited with Ni was dipped into the molten metal and slowly withdrawn under the protection of N_2 against oxidization. Such Si (111 or 101) substrate was located into the center of a horizontal quartz tube. For cleaning the Si surface with N_2, the substrate was heated at 500 ℃ for 10 min under a N_2 flow rate of 100 mL/min. The sealing system was put in the temperature of about 1020 ℃ for 150 min and 900 °C for 60 min which fabricated MCs and MHs, respectively. Ammonia with a flow rate of 60 mL/min or 80 mL/min was run into the furnace for 180 min or 80 min under 0.20 Mpa for MCs or MHs. After the system was cooled down to room temperature, a large piece of products with yellow (MCs) or pale yellow (MHs) were seen in the Si [(111) and (101)] substrates, respectively.

The morphologies and structural properties of the as-prepared GaN samples were investigated by scanning electron microscopy (SEM) (JSM5600LV), transmission electron microscopy (TEM), the energy dispersive X-ray spectroscopy (EDS) (6853-H, Horiba, England), the X-ray powder diffraction (XRD) (D8- Bruker), and Micro-Raman spectra, respectively. TEM samples were prepared using the precision ion beam thinning technology method. The TEM techniques, including high-resolution TEM (HRTEM) and the selected area electron diffraction (SAED), were performed using a Philips FEG TEM CM200 supertwin electron microscope operated at 200 kV. Different temperature photoluminescence (PL) (JY HORIBA FluoroLog-3) measurements were carried with a D_2 (266 nm, 15 mW) laser as an excitation source.

Device Fabrication and Characterization. Similar to our previous work[1], during the fabrication of phosphor-free GaN MC-LED, the undoped GaN MCs were grown firstly on the Si (111) substrate. Subsequently, Mg-doped p-type MC grows naturally as nucleation form on the top of n-type GaN MCs template using a self-assembled CVD system. The growth time was 350 min and there was no

necessary thermal treatment to active Mg. Finally, the metal contacts consist of Ni (20 nm)/Au (200 nm) and Ti (20 nm)/Au (200 nm), which were deposited on p-type conductivity MC surface and the n-type conductivity MC, respectively. The electrodes were prepared by conventional electron-beam lithography and magnetron sputtering technology. The current-voltage (I-V) characteristics were measured using the two probe method after a thermal annealing process for 5 min at 700 °C in a nitrogen atmosphere. I-V characteristics of the devices were measured by a Keithley 4200-SCS electrometer. The EL measurements were carried out by the time resolve electroluminescence spectroscopy with a blaze grating of 500 nm and a scanning step size of 0.5 nm. All the experiments were carried out at room temperature (RT). The measurements were repeated with contacts on various points of each sample to ensure repeatability.

Results and discussion

Figure 1(a, b) depicts the XRD pattern and Micro-Raman spectrum of as-synthesized GaN MCs and MHs at RT. Both typical XRD patterns of the obtained products are shown in Figure 1(a), which are respectively very much matched with standard cubic[23, 37] and wurtzite[10, 38] structures of the GaN crystal, and no peaks of impurity phases are detected. RT Micro-Raman measurements are carried out for GaN [see Figure 1(b)] using green light (514.5 nm) excitation. The E_2 (high) and A_1 (LO) modes of GaN are observed to be consistent with the high crystalline of the pure h-GaN and pure c-GaN, respectively. One for c-GaN at 735.5 cm^{-1} due to A_1 (LO) raman-active phonon mode, while the other matches the h-GaN from E_2 (high) at 567.4 cm^{-1}. As we all know, Raman spectroscopy is also an effective tool for the precise evaluation of stress in GaN epilayers[39]. It is well known that the E_2 (high) mode of h-GaN corresponds to the atomic oscillations in the c-plane and is therefore sensitive to the biaxial stress. In our study, the h-GaN grown on Si (101) is found to have nearly stress-free, as the E_2 phonon peak is nearly no shifted (567.4 cm^{-1}) compared to stress-free bulk hexahedral GaN (567.6 cm^{-1})[39].

Two typical SEM images of as-prepared GaN products for different magnifications were shown in Figure 1 (c, d). Figure 1 (c) reveals high-yield GaN MCs as long as ~7 μm with cross-dimensions in the range of 1.5-2.5 μm. The inset of Figure 1(c) reveals a high-magnification SEM image of the MC which shows clear side facets revealing the characteristics of cubic crystal. The GaN MHs [Figure 1(d)] were observed on the surface of Si (101) substrates. The inset of Figure 1(d) reveals a high-magnification SEM image of a single GaN MH, showing a perfect hexagonal shape with length of

a side of ~ 2 μm and the lengths of 4-5 μm.

Further structure and morphology analyses below confirm that these cube-like microstructures and hexahedron-like microstructures in the SEM images are indeed composed of c-GaN and h-GaN crystals.

The morphology and structure, composition of the GaN MCs or MHs have been characterized in further detail using TEM, HRTEM, and EDS. A typical TEM pattern [Figure 2(a)] of the MC exhibits an obvious rectangle shape consistent with the zinc-blend structure. Figure 2(b) shows the corresponding SAED pattern, the incident beam was parallel to $[001]_{c\text{-}GaN}$ zone axes, which can be seen that the single-crystalline zinc-blende structured GaN crystal. Figure 2(c) is the EDS of MCs, which shows the atomic species Ga and N. The weak carbon peak was considered to be caused by carbon film coated Cu grid that was used to fix the sample onto the sample support during the TEM observations and the Cu element comes from copper mesh. Figure 2(d) shows an HRTEM image of the GaN crystal along the $[001]_{c\text{-}GaN}$ zone axes. The HRTEM [Figure 2(d)] image of the ordered cubic samples standing perpendicular to the substrate which is shows a lattice spacing of 0.45 nm, consistent with the Figure 2(a). In other words, the samples grew in the (111) planes of the substrate Si, which indicate that synthesized of single crystal successfully. As shown in Figure 3(a), clearly reveals that the GaN MHs were composed of hexagonal structure. Subsequently, the corresponding SAED pattern in Figure 3(b), the incident beam was parallel to $[001]_{h\text{-}GaN}$ zone axes, showing the single-crystalline wurtzite structured GaN crystal. Figure 3(c) shows the corresponding EDS of MHs, which can be seen that the atomic species Ga and N. The image in Figure 3(d) which corresponds to the circle part marked in the TEM in Figure 3(a) shows that the clear lattice fringes in this image confirm a single-crystal structure of the MHs. The space of ~0.26 nm between arrowheads corresponds to the distance of (100) planes. Those indicate high intensity in response to pure GaNs synthesized.

In further study, thermodynamical instability of cubic phase GaN and epilayer-substrate chemical incompatibility are some of the key issues bottlenecking such epitaxial deposition schemes[23, 31]. After making an all-around consideration of the various affecting factors including small lattice mismatch and potential applications in optoelectronic devices, Si is an exciting substrate to consider for GaN growth. In this situation, if c-GaN seeds are available, the formation of defects, strains and cracks can be minimized[40]. At the beginning of growth, stacking faults are the main defects to be avoid, and then other defects can be inhibited[32]. Note that the stacking faults are the major factor that supports the

incorporation of h-GaN phase inside the c-GaN. In this case, problems related to drift of the Ga flux and the active nitrogen species, as well as non-uniformity heat distributions towards the surface have become significant at longer period of growth[31, 32]. Under certain optimal flow rate, in other word under ideal III-V (main group elements) ratio, the reaction gas, but not the N_2, dissociates readily on the Si substrate surface yielding atoms needed for the formation of MCs.

Another major challenge for the vapor-liquid-solid (VLS) mechanism is the selection of an appropriate catalyst that leads to the realization of samples. The central role of the catalysts is to form eutectic liquid droplets under proper temperature with the reactants under CVD conditions. The very small miscible droplets of Ni-Ga-N may act as nucleation sites in the VLS growth of GaN MCs[41]. Interestingly, though the TEM and HRTEM, one can conclude that the evidences of the stacking faults are absent. This phenomenon is due to the annihilation of the stacking faults in a larger thickness, whereby these stacking faults disappear by terminating the other stacking faults in different orientations. Through precise control of the growth parameters such as temperature, ammonia flow, and catalyst treatment, the growth was stable and unidirectional, and the ammonia hardly diffuses in any but one direction, producing growth of MCs or MHs only in that direction.

To evaluate the optical characteristics of the GaN MCs formed on the Si (111) substrate, we performed continuous-wave PL measurements. Figure 4 shows the temperature dependence of the PL intensity for the YL band at about 583 nm and band-edge emission at 387 nm in c-GaN MCs. It can be seen that the YL integrated peak intensity decreased, while the band-edge emission intensified in increasing temperature from 150 to 350 K. This is the first observed high performance YL emission in c-GaN. However, the origin of the deep acceptors responsible for YL is still not identified[42-44]. As the origin of the YL band, previous studies on GaN have claimed that carbon-related impurity and dislocation densities are responsible for the well-known YL band centered at 2.1−2.3 eV[24, 42, 45-47]. The other proposed models involve transitions from shallow donors to either deep acceptors or deep donors, or from deep double donors to shallow acceptors have attracted attention as a candidate[48-54]. Form the image in Figure 2(a) and the FWHM in HRXRD rocking curve of GaN MCs (Supporting information) with a low density of threading dislocations; it is clear that dislocation defects can be ruled out by the effect of the YL. As shown in Figure 4, the intensity of the YL emission is even higher than that of the band-edge emission at 150 K, while the emissions from the YL emissions are almost suppressed when the temperature was 250 K or higher, and the prominent peak at 387 nm is the only dominant peak at

350 K(see in Figure 4). From the temperature dependence of the PL, we find that the YL is due to shallow-to-deep donor recombination[55]. The results manifest a strong correlation in properties related to deep levels. All the above-mentioned structural and componential analyses clearly reveal that our designed CVD method can successfully synthesize single crystalline structure GaN MCs with high purity, and the as-grown GaN MCs could be considered to assemble low-dimensional prototype optoelectronic devices.

Utilizing the as-grown GaN MCs, a low-dimensional structure LED is fabricated. In order to evaluate the electrical properties of the MC-LED with highly crystalline nature, we have adapted an assembly fabrication by choosing a single MC. First, we have separated MCs from the Si (111) substrate by using sonication. Subsequently, an individual MC was chosen on the electrode grid and then assembly fabrication of the MC was performed by using focused ion beam on a SiO_2 coated Si substrate. Figure 5 shows the schematic structure of the assembly fabrication, where the homojunction MC lies with a length of about 4 μm on the Si substrate surface and about 1 μm embedded in the two electrodes films. The I-V curve of the individual phosphor-free white MC-LED device is illustrated in Figure 6(a). Obviously, the I-V curve of exponential relationship shows diode nonlinear rectification characteristics with a turn-on voltage of about 5 V. The homojunction behaves like an efficient diode with a current increasing rapidly under forward bias and blocking the current flow under reverse bias till -15 V. The linear curves in the inset of Figure 6(a) for both Au/Ti/n-GaN and Au/Ni/p-GaN indicate that the ohmic contacts have been realized. Also, the two metal semiconductor contacts showing good ohmic contact are revealed in the I-V measurements after the rapid thermal annealing treatments individually, indicating that the rectifying behavior originated from the GaN homojunction.

To probe optoelectronic properties of the single p-n homostructured GaN MCs, the EL spectra of the single homojunction MC-LED under various operating voltages ranging from 0 to 15 V at RT are systematically investigated and exhibited in Figure 6(b). The EL spectra are composed of two emission peaks in the blue and yellow regions, respectively. The blue peak locates at around 453 nm, while the yellow one is around 595 nm. It is obvious that the shape of the EL spectra change with the applied voltage increase. When the applied voltage level is 0 V, the blue and yellow component of the spectrums could hardly be observed. In the range of applied voltage from 3 to 9 V, the intensity of two EL emission peaks at 453 and 595 nm are both increased, and the integrated intensity ratio of the blue and yellow peaks is 0.02 and the color of the device is yellow. When the applied voltage is 12 V, the

integrated intensity ratio of the two emission components is 0.51. In this situation, the EL spectrum corresponded to a white-light source derives the Commission Internationale de I'Eclairage (CIE) chromaticity coordinates. The inset is the emitting image of the single p-n homojunction at 12 V. However, as the applied voltage increased, the intensity of the blue peak became stronger while the yellow peak became weaker. The color of the device is blue at 15 V. As a whole, Figure 6(b) shows that the two EL peaks shift towards higher energy side at increased applied voltage due to screening of the small polarization field by injected carriers. The excellent luminescent properties of the phosphor-free LED imply the potential application on micro/nanoscale light source based on c-GaN. In addition, the high brightness light emission from p-n c-GaN homojunctions can also be observed after three months, revealing the high stability of our phosphor-free MC-LED devices in ambient.

The absolute output power of the devices is measured by using an integrating sphere. It is worthwhile mentioning that no electron blocking layers were incorporated in the device active regions. Figure 7(a) shows the light output power curves of single MC-LED and conventional single p-n h-GaN homojunction LED (MH-LED) on Si substrates as a function of injection current. It can be noted that for both samples, the light output power increases monotonously with the increase in injection current. For LED based on MC, even when the injection current increases to 100 mA, the light output power still exhibits an upward trend without saturation, indicating excellent electronic properties which are comparable to the conventional MH-LED. On the other hand, the light output power of MC-LED was enhanced by approximately 50% for a typical operating current of 20 mA compared with that of conventional MH-LED. To the best of our knowledge, this is the highest power ever reported for any micro/nanostructure GaN-based phosphor-free white LEDs. We suggest the mechanism of the efficiency enhancement associated with MC is due to the increased IQE caused by the reduction of threading dislocation density, and the absence of piezoelectric polarization of the zinc-blend phase GaN.

The LED luminous efficiency (η_{LED}), as given by below equation, is mainly comprised of the resistive losses due to Joule heating, injection losses, and IQE. The IQE describes the fraction of the available carriers (N) that recombines radiatively which described by the BN^2 term. The dominating nonradiative processes which defined by the AN term are defect-mediated recombination and the Auger recombination in which electron-hole recombination energy is dissipated to other carriers rather than emitted as a photon (described by the CN^3 term)[56].

$$\eta_{LED} = \eta_{Joule} \cdot \eta_{Injection} \cdot \frac{BN^2}{AN + BN^2 + CN^3}$$

Although all the components are important, efficiencies of the state-of-the-art devices today are mainly determined by injection efficiency and IQE[57]. The doped p-type layers were modulated using Mg to enhance the hole injection and transport process. The stable emission is attributed to a negligible quantum-confined Stark effect and the enhanced hole transport, due to p-type modulation doping. The IQE is the number of photons generated from an electron−hole pair injected into LEDs, that is, the ability of the semiconductor LED to convert electricity into light. The single MC-LED and MH-LED are measured under pulsed current-injection mode to eliminate Joule heating. Figure 7(b) plots the IQE as a function of the forward current for the individual MC-LED and MH-LED, respectively. The IQE first increases with increasing injection currents for both types of devices and shows virtually no efficiency droop as the injection current increases. It reaches the maximum values of 99.2% and 95.0% at ~72.0 and 73.7 mA, for the zinc-blende and wurtzite phase devices, respectively. These values are significantly higher than the IQE of any previously reported white micro/nanostructure LEDs[7, 58]. More importantly, with the use of zinc-blende phase GaN, the IQE shows a more than 50% increase, which the most efficient phosphor-free white LEDs ever reported.

The high threading dislocations density would give rise to numerous nonradiative recombination sites and scattering centers, which causes a large decrease in IQE, deteriorating the electrical and optical characteristics of GaN-based devices. Through the studies of the dislocation density of the GaN samples by a HRXRD rocking curve (See supporting information), compared to the previous reports[59, 60], c-GaN with a low dislocation density < 10^8 cm^{-2} is highly desirable because it can increase the lifetime for continuous operation of diodes. This ultralow dislocation density which suppressed nonradiative recombination contributes to high-performance MC-LED with a higher light emission efficiency compared with a conventional h-GaN. Obviously, the improvement of heteroepitaxial GaN quality to achieve a lower dislocation density is a crucial issue[61].

The enhanced emission efficiency and no efficiency droop as the injection current increases are also attributed to the absence of piezoelectric polarization of the zinc-blend phase GaN MC-LED. It is well-known that the piezoelectric field will cause a spatial separation of the electron and hole wave functions as well as a reduction of the radiative recombination rate[33, 62, 63]. In other words, in the case of LED based on c-GaN, the piezoelectric field effect did not occur due to the noninfluence of

polarization. Nonpolar LED may also benefit from enhanced carrier injection efficiency due to the absence of internal polarization-related electric fields that result in a "sawtooth" energy band profile that impacts carrier transport through the quantum-confined stack[64]. Because of this phenomenon, the efficiency improved in zinc-blend MC-LEDs. Our results demonstrate that the fabricated nonpolar MC-LEDs are remarkable and can improve the efficiency of the LED.

Conclusions

In conclusion, large area zinc-blende phase with high-performance yellow-band emission GaN MCs were synthesized by CVD method. Studies on the single c-GaN homojunction phosphor-free LED show excellent white emission under an operating voltage of 12 V. We have demonstrated the most efficient phosphor-free white MC-LEDs ever reported, which exhibit an internal quantum efficiency of ~99.2% and an output power of ~4.4 mW for a typical operating current of 20 mA, which is more than 50% stronger than that of conventional h-GaN homojunction LED. The photoelectrical properties of MC-LEDs exhibit superior luminous and power efficiency to that of MH-LED owing to the ultralow dislocation density and the absence of piezoelectric polarization. The polarization-free MC-LEDs also show many desired properties, including highly stable white light emission, that are ideally suited for next-generation LEDs. This work constitutes significant progress for achieving low-cost, high-performance phosphor-free white LEDs utilizing polarization-free MCs.

Acknowledgements

This work is partially financially supported by the National Natural Science Foundation of China (Grants 21371049 and 20971036).

Notes and references

1. X.B. Tang, G.M. Li and S.M. Zhou, *Nano Lett.*, 2013, **13**, 5046-5050.
2. C.T. Huang, J. Song, W.F. Lee, Y. Ding, Z. Gao, Y. Hao, L.J. Chen and Z.L. Wang, *J. Am. Chem. Soc.*, 2010, **132**, 4766-4771.
3. X. Tang, S. Zhou and X. Yuan, *Mater. Lett.*, 2013, **93**, 25-27.
4. X. Zhang, W. Liu, G.Z. Wei, D. Banerjee, Z. Hu and J. Li, *J. Am. Chem. Soc.*, 2014, **136**, 14230-14236.
5. S. Jahangir, I. Pietzonka, M. Strassburg and P. Bhattacharya, *Appl. Phys. Lett.*, 2014, **105**, 111117.
6. H.P. Nguyen, S. Zhang, A.T. Connie, M.G. Kibria, Q. Wang, I. Shih and Z. Mi, *Nano Lett.*, 2013, **13**,

5437-5442.
7. H.P. Nguyen, K. Cui, S. Zhang, M. Djavid, A. Korinek, G.A. Botton and Z. Mi, *Nano Lett.*, 2012, **12**, 1317-1323.
8. X. Duan and C.M. Lieber, *J. Am. Chem. Soc.*, 2000, **122**, 188-189.
9. T. Douglas and N.C.Yong, *Adv. Funct. Mater.*, 2006, **16**, 1197-1202.
10. C.C. Chen, C.C. Yeh, C.H. Chen, M.Y. Yu, H.L. Liu, J.J. Wu, K.H. Chen, L.C. Chen, J.Y. Peng and Y.F. Chen, *J. Am. Chem. Soc.*, 2001, **123**, 2791 -2798.
11. H. Morkoc and S. N. Mohammad, *Science*, 1995, **267**, 51-55.
12. K. Chung, C.H. Lee, and G.C. Yi, *Science*, 2010, **330**, 655-657.
13. H.P. Nguyen, S. Zhang, K. Cui, X. Han, S. Fathololoumi, M. Couillard, G.A. Botton and Z. Mi, *Nano Lett.*, 2011, **11**, 1919-1924.
14. X. Ren, X. Zhang, N. Liu, L. Wen, L. Ding, Z. Ma, J. Su, L. Li, J. Han and Y. Gao, *Adv. Funct. Mater.*, 2015, **25**, 2182-2188.
15. D.I. Son, B.W. Kwon, D.H.Park, W.S. Seo, Y. Yi, B. Angadi, C.L. Lee, and W.K. Choi, *Nat. Nanotechnology*, 2012.71, 1-7.
16. P.Siddha,and S. Nakamura, *Nat.Photo.*, 2009, **3**, 180-182.
17. S.F. Chichibu, A. Uedono, T. Onuma, B.A. Haskell, A. Chakraborty, T. Koyama, P.T. Fini, S. Keller, S.P. Denbaars, J.S. Speck, U.K. Mishra, S. Nakamura, S. Yamaguchi, S. Kamiyama, H. Amano, I. Akasaki, J. Han and T. Sota, *Nat. Mater.*, 2006, **5**, 810-816.
18. I. Akasaki and H. Amano, *Jap. J.Appl. Phys.*, 2006, **45**.
19. X. Xiang, C. Cao, Y. Xu and H. Zhu, *Nanotechnology*, 2006, **17**, 30-34.
20. J. Hu, Y. Bando, J. Zhan, F. Xu, T. Sekiguchi and D. Golberg, *Adv. Funct. Mater.*, 2004, **16**, 1465-1469.
21. S.H.Park,and S.L. Chuang, *Appl. Phys. Lett.*, 2000, **87**, 355-364.
22. S.R. Xu, Y. Hao, J.C. Zhang, Y.R. Cao, X.W. Zhou, L.A. Yang, X.X. Ou, K. Chen and W. Mao, *J. Cryst. Growth*, 2010, **312**, 3521-3524.
23. C. Bayram, J.A. Ott, K.T. Shiu, C.W. Cheng, Y. Zhu, J. Kim, M. Razeghi and D.K. Sadana, *Adv. Funct. Mater.*, 2014, **24**, 4492-4496.
24. S. Xu, Y. Hao, J. Zhang, T. Jiang, L. Yang, X. Lu and Z. Lin, *Nano Lett.*, 2013, **13**, 3654-3657.
25. M.C. Chou, D.R. Hang, L. Chang, C. Chen, W.F. Yang, C.A. Li and J.J. Wu, *J. Appl. Phys.*, 2010, **107**, 013502.
26. X.L. Sun, H. Yang, L.X. Zheng, D.P. Xu, J.B. Li and Y.T. Wang, *Appl. Phys. Lett.*, 1999, **74**.
27. B.M. Shi, M.H. Xie, H.S. Wu, N. Wang and S.Y. Tong, *Appl. Phys. Lett.*, 2006, **89**, 151921.
28. H. Amano and A.I. Sawaki N, *Appl. Phys. Lett.*, 1986, **48**, 353-355.
29. C.H. Wei, Z.Y. Xie, L.Y. Li, Q.M. Yu and J.H. Edgar, *J. Electron. Mater.*, 2000, **29**, 317-321.
30. H. Vilchis and A. Escobosa, *Thin Solid Films*, 2012, **520**, 5191-5194.
31. S.V. Novikov, N.M. Stanton, R.P. Campion, R.D. Morris, H.L. Geen, C.T. Foxon and A.J. Kent, *Semicond. Sci. Technol.*, 2008, **23**, 015018.
32. R.M. Kemper, M. Weinl, C. Mietze, M. Häberlen, T. Schupp, E. Tschumak, J.K.N. Lindner and K. Lischka, *J. Cryst. Growth*, 2011, **323**, 84-87.
33. M.H. Kim, M.F. Schubert, Q. Dai, J.K. Kim, E.F. Schubert, J. Piprek and Y. Park, *Appl. Phys. Lett.*, 2007, **91**, 183507.
34. S. Inoue, K. Okamoto, N. Matsuki, T.W. Kim, and H. Fujioka, *Appl. Phys. Lett.*, 2006, **88**, 1-3.
35. E. Martinez-Guerrero, C. Adelmann, F. Chabuel, J. Simon, N.T. Pelekanos, G. Mula, B. Daudin, G. Feuillet and H. Mariette, *Appl. Phys. Lett.*, 2000, **77**, 809-811.
36. S.M. Zhou, H.C. Gong, B. Zhang, Z.L. Du, X.T. Zhang and S.X. Wu, *Nanotechnology*, 2008, **19**, 175303.

37. Y. Xie, Y. Qian, W. Wang, S. Zhang and Y. Zhang, *Science*, 1996, **272**.
38. V. Purushothaman and K. Jeganathan, *J.Phys. Chem. C*, 2013, **117**, 7348-7357.
39. A.H. Park, T.H. Seo, S. Chandramohan, G.H. Lee, K.H. Min, S. Lee, M.J. Kim, Y.G. Hwang and E.K. Suh, *Nanoscale*, 2015, **7**, 15099-15105.
40. S.N. Waheeda, N. Zainal, Z. Hassan, S.V. Novikov, A.V. Akimov and A.J. Kent, *Appl. Surf. Sci.*, 2014, **317**, 1010-1014.
41. C.C. Chen and C.C. Yeh, *Adv. Mater.*, 2000, **10**, 738-741.
42. S.G. Christenson, W. Xie, Y. Sun and S.B. Zhang, *J. Appl. Phys.*, 2015, **118**, 135708.
43. D.O. Demchenko, I.C. Diallo and M.A. Reshchikov, *Phys. Rev. Lett.*, 2013, **110**.
44. S. Ito, T. Nakagita, N. Sawaki, H.S. Ahn, M. Irie, T. Hikosaka, Y. Honda, M. Yamaguchi and H. Amano, *Jap. J. Appl. Phys.*, 2014, **53**, 11RC02.
45. X. Li, P.W. Bohn and J.J. Coleman, *Appl. Phys. Lett.*, 1999, **75**, 4049.
46. M. A. Reshchikov, *Appl. Phys. Lett.*, 2006, **89**, 232106.
47. J.L. Lyons, A. Janotti and C.G. Van de Walle, *Appl. Phys. Lett.*, 2010, **97**, 152108.
48. T. Suski, P. Perlin, H. Teisseyre, M. Leszczyński, I. Grzegory, J. Jun, M. Boćkowski, S. Porowski and T.D. Moustakas, *Appl. Phys. Lett.*, 1995, **67**, 2188.
49. J.R. Neugebauer and C.G. Van de Walle, *Appl. Phys. Lett.*, 1996, **69**, 503.
50. G. Li, S.J. Chua, S.J. Xu, W. Wang, P. Li, B. Beaumont and P. Gibart, *Appl. Phys. Lett.*, 1999, **74**, 2821.
51. M.A. Reshchikov, H. Morkoç, S.S. Park and K.Y. Lee, *Appl. Phys. Lett.*, 2001, **78**, 3041.
52. H.Y. Huang, C.H. Chuang, C.K. Shu, Y.C. Pan, W.H. Lee, W.K. Chen, W.H. Chen and M.C. Lee, *Appl. Phys. Lett.*, 2002, **80**, 3349.
53. J. Mickevičius, R. Aleksiejūnas, M.S. Shur, S. Sakalauskas, G. Tamulaitis, Q. Fareed and R. Gaska, *Appl. Phys. Lett.*, 2005, **86**, 041910.
54. F.J. Xu, B. Shen, L. Lu, Z.L. Miao, J. Song, Z.J. Yang, G.Y. Zhang, X.P. Hao, B.Y. Wang, X. Q. Shen and H. Okumura, *J. Appl. Phys.*, 2010, **107**, 023528.
55. S.J. Chung, O.H. Cha, Y.S. Kim, C.H. Hong, H.J. Lee, M.S. Jeong, J.O. White and E.K. Suh, *J. Appl. Phys.*, 2001, **89**, 5454.
56. T.R. Kuykendall, A.M. Schwartzberg and S. Aloni, *Adv. Mater.*, 2015, **27**, 5805-5812.
57. H.P.T. Nguyen, S. Zhang, A.T. Connie, M.G. Kibria, Q. Wang, I. Shih and Z. Mi, *Nano Lett.*, 2013, **13**, 5437-5442.
58. S.M. Sadaf, Y.H. Ra, H.P. Nguyen, M. Djavid and Z. Mi, *Nano Lett.*, 2015, **15**, 6696-6701.
59. W. Wang, H. Yang and G. Li, *J. Mater. Chem. C*, 2013, **1**, 4070.
60. L. Zhang, X. Li, Y. Shao, J. Yu, Y. Wu, X. Hao, Z. Yin, Y. Dai, Y. Tian, Q. Huo, Y. Shen, Z. Hua and B. Zhang, *ACS Appl Mater Interfaces*, 2015, **7**, 4504-4510.
61. H.Y. Shih, M. Shiojiri, C.H. Chen, S.F. Yu, C.T. Ko, J.R. Yang, R.M. Lin and M.J. Chen, *Sci Rep*, 2015, **5**, 13671.
62. C.H. Cheng, A.J. Tzou, J.H. Chang, Y.C. Chi, Y.H. Lin, M.H. Shih, C.K. Lee, C.I. Wu, H.C. Kuo, C.Y. Chang and G.R. Lin, *Sci Rep*, 2016, **6**, 19757.
63. H. Jeong, S.Y. Jeong, D.J. Park, H.J. Jeong, S. Jeong, J.T. Han, H.J. Jeong, S. Yang, H.Y. Kim, K.J. Baeg, S.J. Park, Y.H. Ahn, E.K. Suh, G.W. Lee, Y.H. Lee and M.S. Jeong, *Sci Rep*, 2015, **5**, 7778.
64. A.M. Armstrong, K. Kelchner, S. Nakamura, S.P. DenBaars and J.S. Speck, *Appl. Phys. Lett.*, 2013, **103**, 232108.

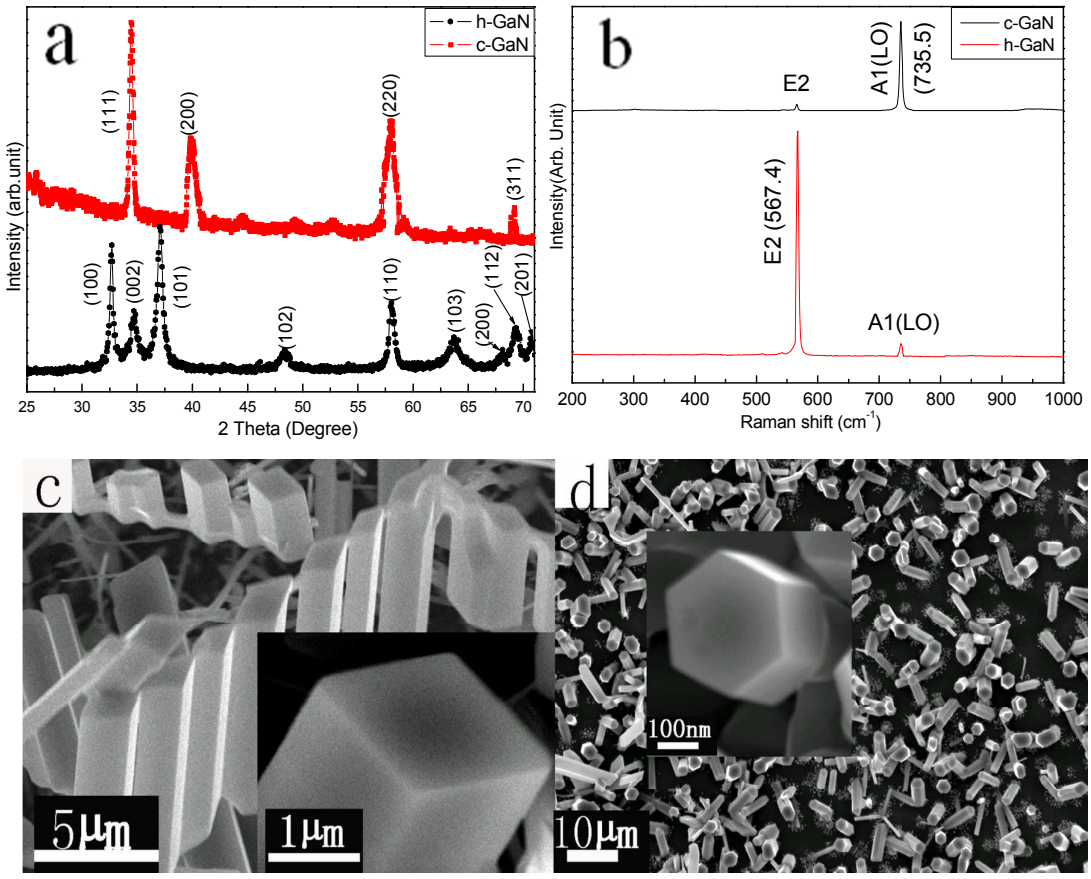

Figure 1 **(a)** The XRD spectra of MCs and MHs. **(b)** Room temperature Micro-Raman spectra of GaN MCs and GaN MHs. **(c),(d)** the SEM images of GaN MCs or MHs.

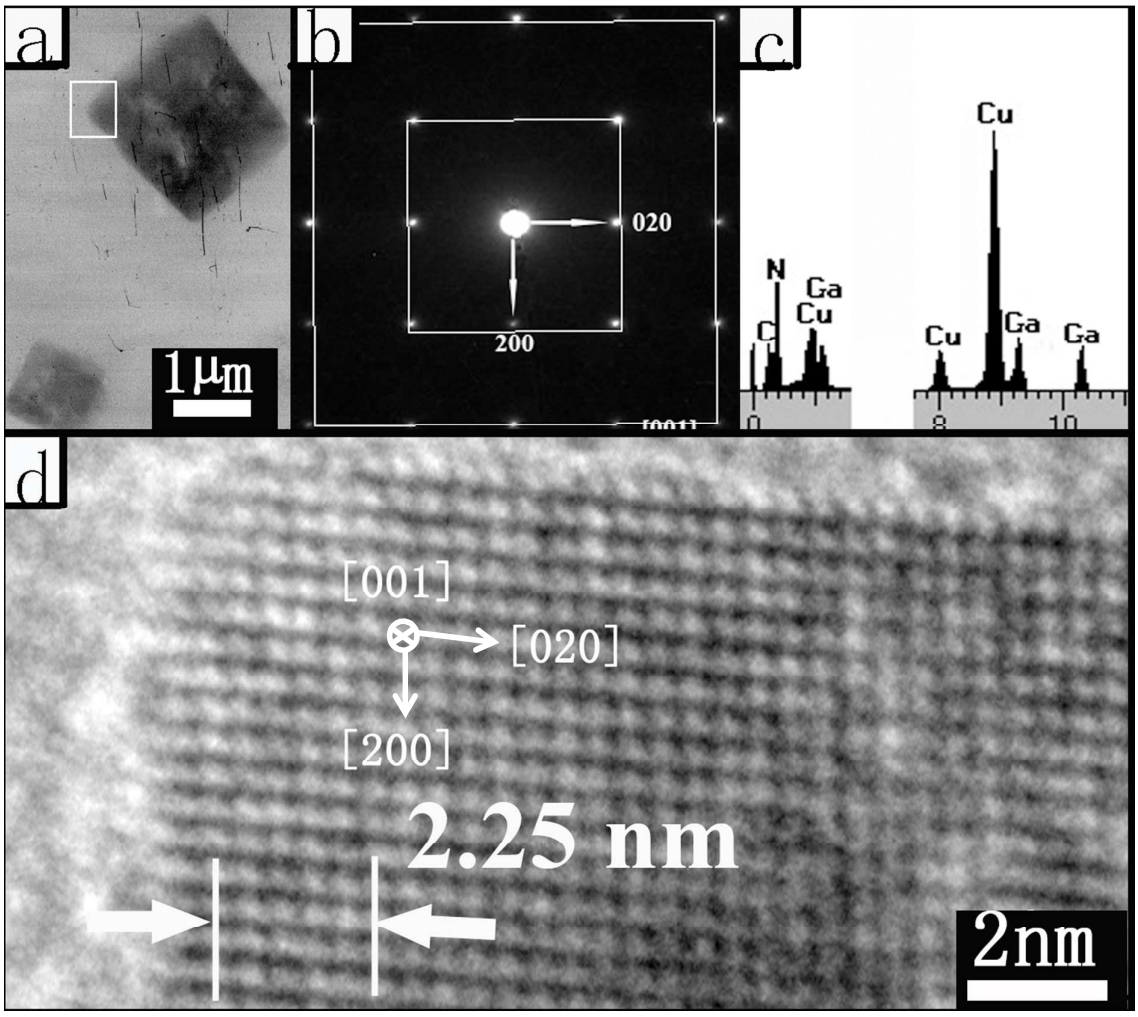

Figure 2 the image of synthetic GaN MCs (a) TEM, (b) SAED, (c) EDS, (d) HRTEM

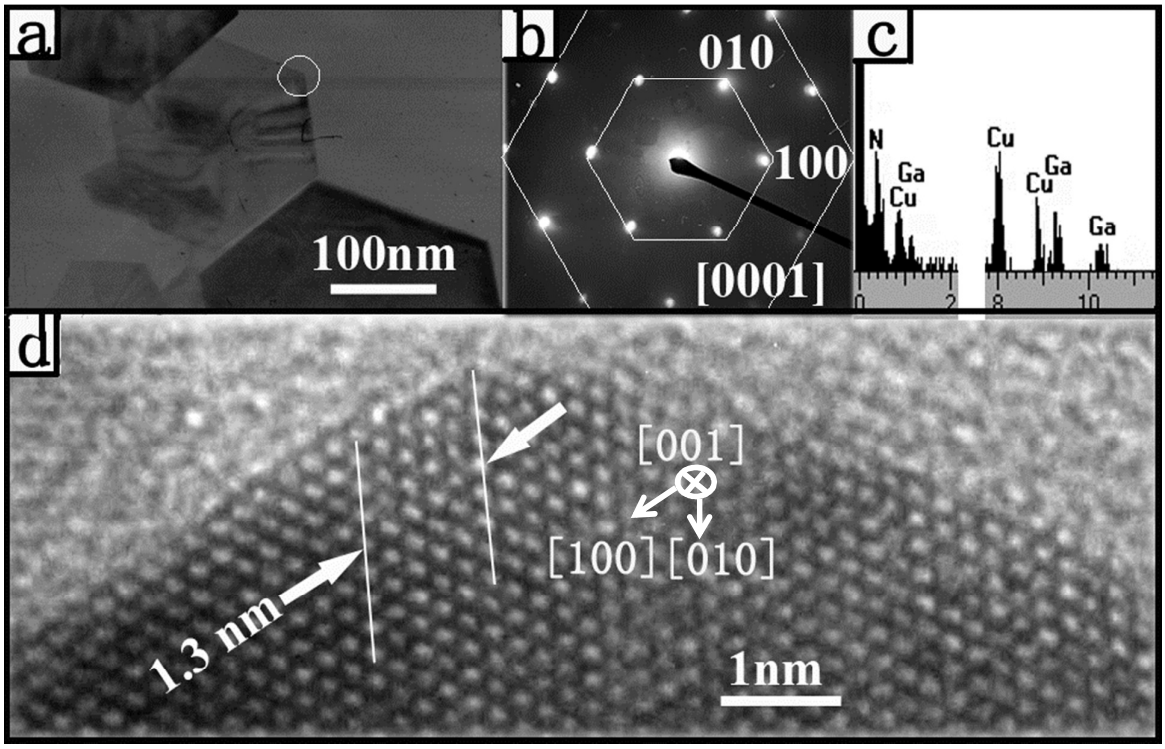

Figure 3 The as-synthesized GaN MHs (a) TEM, (b) SAED, (c) EDS, (d) HRTEM

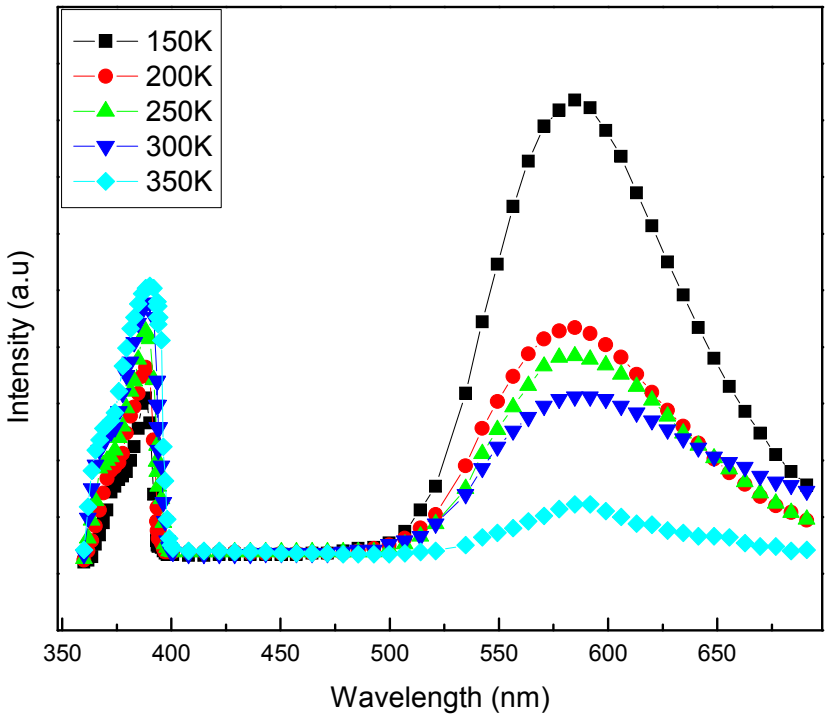

Figure 4 Different temperature PL spectra of GaN MCs.

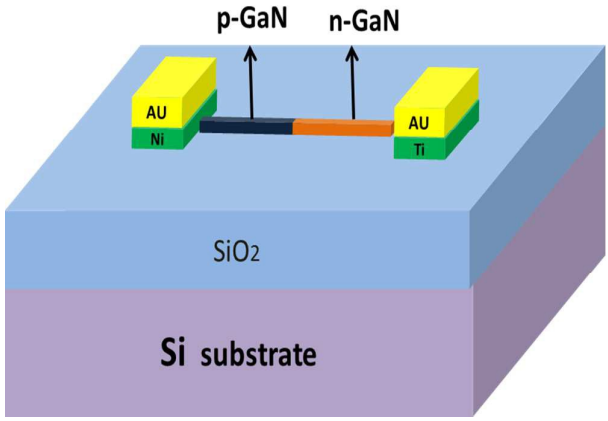

Figure 5 Schematic test illustration of the p-n homojunction GaN MC LED device.

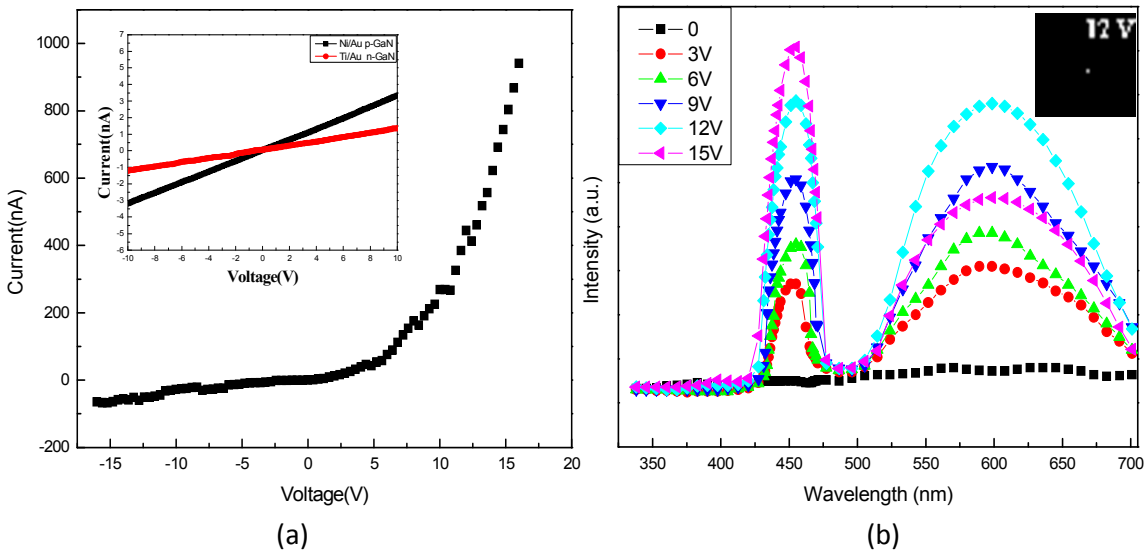

Figure 6 (a) I−V curves of the homojunction diode (inset: the ohmic contact characteristics of the electrodes). (b) EL spectra of the p-n c-GaN in various operating voltage conditions at RT (inset: the emitting image of the individual p-n homojunction at 12V).

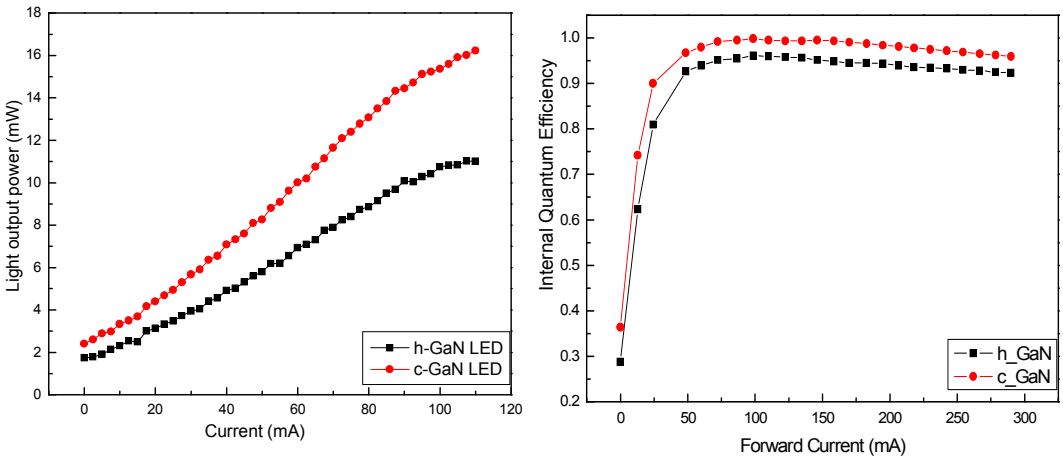

Figure 7 (a) The light output power curves of the single MC-LED and MH-LED as a function of injection current. (b) Variations of the relative IQE with injection current for the emission from the individual MC-LED and MH-LED measured at room temperature.